

SCIENTIFIC REPORTS



OPEN

Generation of steady entanglement via unilateral qubit driving in bad cavities

Zhao Jin¹, Shi-Lei Su², Ai-Dong Zhu³, Hong-Fu Wang³, Li-Tuo Shen⁴ & Shou Zhang^{1,3}

We propose a scheme for generating an entangled state for two atoms trapped in two separate cavities coupled to each other. The scheme is based on the competition between the unitary dynamics induced by the classical fields and the collective decays induced by the dissipation of two non-local bosonic modes. In this scheme, only one qubit is driven by external classical fields, whereas the other need not be manipulated via classical driving. This is meaningful for experimental implementation between separate nodes of a quantum network. The steady entanglement can be obtained regardless of the initial state, and the robustness of the scheme against parameter fluctuations is numerically demonstrated. We also give an analytical derivation of the stationary fidelity to enable a discussion of the validity of this regime. Furthermore, based on the dissipative entanglement preparation scheme, we construct a quantum state transfer setup with multiple nodes as a practical application.

Quantum entanglement is an intriguing property of composite systems. The term refers to inseparable correlations that are stronger than all classical counterparts^{1,2}. To perform quantum communication safely and perfectly, remote parties are usually required to share a quantum channel of a maximally entangled state. Nevertheless, in real experiments, it is difficult to achieve a perfect quantum channel due to environmental noise. Therefore, in long-distance quantum communication and quantum communication networks, the generation of a steady entanglement between different nodes is significantly challenging^{3,4}. The main obstacle in preserving entanglement is dissipation induced by the environment, which is inevitable in the development of quantum science and technology. Generally, entanglement purification^{5,6}, together with the use of quantum repeaters^{7,8}, is an efficient method for addressing environmental noise. From this perspective, it seems rather conflicting that dissipation can be used as a powerful resource to create entanglement^{9–40} or to realize a spin squeezing state^{41,42}. In 1999, Plenio *et al.* and Cabrillo *et al.* presented schemes for engineering entanglement that utilize dissipation^{9,10}, which opened up a new chapter for entanglement generation based on dissipative dynamics. Afterward, several schemes were suggested for studying the entanglement in dissipative quantum systems. In particular, Kastoryano, Reitor, and Srensen considered a dissipative scheme for preparing a maximally entangled state of two Λ -type atoms in a high-finesse optical cavity¹¹. Their results were better than those obtained via unitary-dynamics-based schemes, as their schemes do not require specifying the initial state or accurately controlling the evolution time. Shen *et al.* generalized this scheme to prepare distributed entanglement via dissipation^{12,13}. In addition, Reiter *et al.*¹⁴ proposed a dissipative scheme in which two transmon qubits can be driven into a steady state in a circuit quantum electrodynamics setup. Recently, the dissipative generation of steady entanglement between two qubits was experimentally achieved using trapped ions^{35,36} and superconducting qubits³⁷. Moreover, several interesting schemes concerning the manipulation of quantum states with dissipation dynamics exist, such as the dissipation-induced geometric phase⁴³, stimulated Raman adiabatic passage (STIRAP) via dissipative quantum dynamics⁴⁴, and dissipation-assisted quantum state manipulation in cavities⁴⁵.

To perform large-scale quantum computing, the quantum control of separate nodes of a quantum network is indispensable. Coupled cavities are an essential aspect of distributed quantum information processing. One important step is to entangle qubits located in spatially separated resonators. To date, several theoretical^{46–53} and experimental schemes⁵⁴ for generating maximally entangled states have been proposed. Most of these schemes

¹Department of Physics, Harbin Institute of Technology, Harbin, 150001, China. ²School of Physical Science Engineering and Key Laboratory of Materials Physics of Ministry of Education of China, Zhengzhou University, Zhengzhou, 450052, China. ³Department of Physics, College of Science, Yanbian University, Yanji, Jilin, 133002, China. ⁴Laboratory of Quantum Optics, Department of Physics, Fuzhou University, Fuzhou, 350002, China. Correspondence and requests for materials should be addressed to S.Z. (email: szhang@ybu.edu.cn)

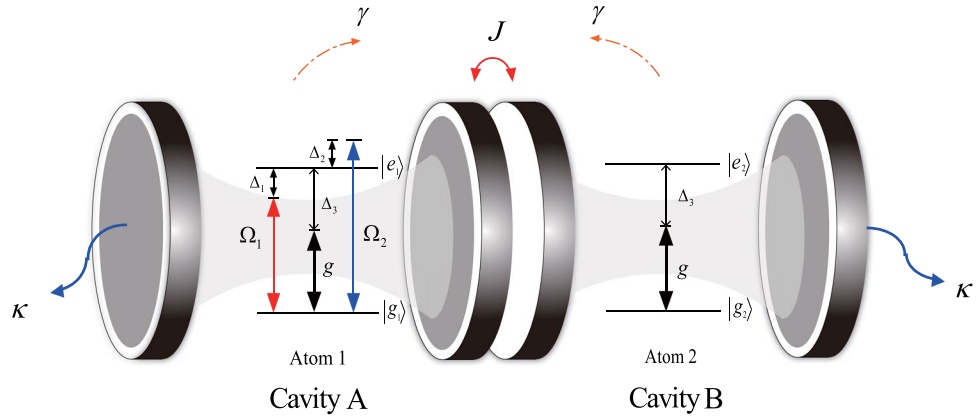


Figure 1. Experimental setup for engineering an entangled steady state for two identical two-level atoms via dissipation in two directly coupled cavities. Two quantized cavity fields are dispersively coupled to the qubits with detuning Δ_3 and coupling strength g . Two off-resonance optical lasers with detuning Δ_k and Rabi frequency Ω_k ($k = 1, 2$) simultaneously drive the first atom. γ and κ are the atomic spontaneous emission rate and the cavity decay rate, respectively.

focus on unitary dynamical evolution, in which the inevitable noise can have only detrimental effects, and the system requires precise time control and state initialization.

In this paper, we propose a scheme for preparing and stabilizing a maximally entangled state in coupled cavities by effectively utilizing the unitary dynamics provided by microwave fields and the dissipation originating from cavity decay, where only one atom is driven by two classical fields with precisely chosen frequencies. Our present work has the following features: (i) Our scheme performs well without the need to specify the initial state nor control the evolution time accurately. (ii) This scheme applies unilateral classical driving to only one atom. This is in contrast to ref.²⁷, in which both atoms must be driven by three optical lasers. Finally, (iii) our scheme can be generalized to multiple-coupled-cavity models to perform quantum processing tasks such as state transfer between separate nodes. With the currently achievable experiment parameters, the numerical simulation demonstrates that steady-state entanglement with high fidelity, purity, and Clauser-Horne-Shimony-Holt (CHSH) correction can be obtained⁵⁵ and that the scheme is robust against parameter fluctuations. We also give an analytical form of the fidelity to demonstrate the validity of our scheme.

Results

Theoretical Model. The coupled-cavity system under consideration is shown in Fig. 1. Two identical two-level atoms 1 and 2 are trapped in two coupled cavities. Each atom has a ground state $|g\rangle$ and an excited state $|e\rangle$, with the corresponding energies 0 and ω_0 . The atomic transition $|g_i\rangle \leftrightarrow |e_i\rangle$ ($i = 1, 2$) is dispersively coupled to the cavity mode with the coupling constant g and detuning Δ_3 , and the first atom is driven by two off-resonance optical lasers with Rabi frequency Ω_k and detuning Δ_k ($k = 1, 2$). Photons can hop between the cavities. The Hamiltonian of the system can be written as (setting $\hbar = 1$ throughout this paper) $H = H_{WL} + H_{CL}$, with

$$H_{WL} = \sum_{i=1,2} \omega_0 |e_i\rangle \langle e_i| + \sum_{j=A,B} \omega_a a_j^\dagger a_j + J(a_A^\dagger a_B + a_A a_B^\dagger) + [g(S_1^\dagger a_A + S_2^\dagger a_B) + \text{H.c.}], \quad (1)$$

$$H_{CL} = \sum_{k=1,2} \Omega_k e^{-i\omega_k t} S_1^\dagger + \text{H.c.}, \quad (2)$$

where $S_i^\dagger = |e_i\rangle \langle g_i|$ ($i = 1, 2$); $|e_i\rangle$ and $|g_i\rangle$ are the excited and ground states of the i th qubit, respectively; a_j and a_j^\dagger denote the annihilation and creation operators for the optical mode of cavity j , respectively; Ω_k and ω_k represent the amplitude and frequency of the k th driving field, respectively; ω_a denotes the frequency of the cavity mode; and J is the photon-hopping strength, which describes the coupling between two cavities. To simplify the dynamics of the system, we introduce the non-local bosonic modes

$$\begin{aligned} c_1 &= \frac{\sqrt{2}}{2}(a_A + a_B), \\ c_2 &= \frac{\sqrt{2}}{2}(a_A - a_B). \end{aligned} \quad (3)$$

These two modes are not coupled with each other and are linearly related to the field modes of the two cavities. In terms of the new operators, the Hamiltonian H_{WL} can be rewritten as

$$H_{WL} = \sum_{i=1,2} \omega_0 |e_i\rangle \langle e_i| + (\omega_a + J)c_1^\dagger c_1 + (\omega_a - J)c_2^\dagger c_2 + \frac{g}{\sqrt{2}}[S_1^\dagger(c_1 + c_2) + S_2^\dagger(c_1 - c_2) + \text{H.c.}]. \quad (4)$$

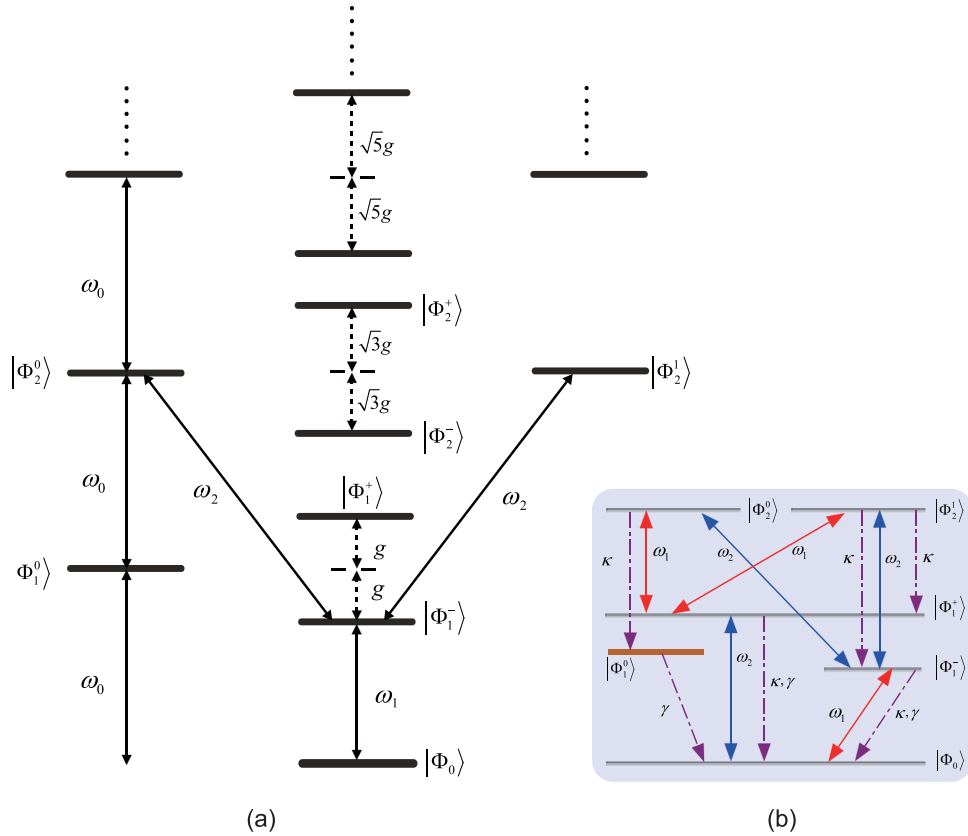


Figure 2. (a) Level configuration in the dressed state picture. (b) Processes for producing and stabilizing Bell states. The interaction between the system and the environment is characterized by photon loss and atomic spontaneous emission, with rates κ and γ , respectively.

The Hamiltonian H_{WL} describes the coupling of the two atoms to the delocalized field modes c_1 and c_2 with frequencies $\omega_a + J$ and $\omega_a - J$. In the interaction picture with respect to $H_0 = \sum_{i=1,2} \omega_0 |e_i\rangle\langle e_i| + (\omega_a + J)c_1^\dagger c_1 + (\omega_a - J)c_2^\dagger c_2$, we obtain the interaction Hamiltonian

$$H_{WL}^I = \frac{\sqrt{2}}{2} g e^{i\Delta_3 t} [(e^{-ijt} c_1 + e^{ijt} c_2) S_1^\dagger + (e^{-ijt} c_1 - e^{ijt} c_2) S_2^\dagger + \text{H.c.}], \tag{5}$$

in which $\Delta_3 = \omega_0 - \omega_a$. Meanwhile, bosonic mode c_1 is resonant with the two qubits, and bosonic mode c_2 is largely dispersive with the two qubits under the conditions of $J = \Delta_3$ and $\Delta_3 + J \gg g$. Therefore, after discarding the rapidly oscillating terms, the interaction Hamiltonian reduces to

$$H_{WL}^I = \frac{\sqrt{2}}{2} g (S_1^\dagger + S_2^\dagger) c_1 + \text{H.c.} \tag{6}$$

The dynamics of an open dissipative system in Lindblad form is described by the master equation

$$\dot{\rho}(t) = i[\rho(t), H] + \frac{1}{2} \sum_j \left[2\hat{L}_j \rho(t) \hat{L}_j^\dagger - (\hat{L}_j^\dagger \hat{L}_j \rho(t) + \rho(t) \hat{L}_j^\dagger \hat{L}_j) \right], \tag{7}$$

where H represents the original Hamiltonian of the whole system, as shown in Eqs (1) and (2), and the Lindblad superoperator is defined as \hat{L}_j . Specifically, in the current scheme, the Lindblad operators can be expressed as $\hat{L}_{\kappa i} = \sqrt{\kappa} a_i$ ($i = A, B$), which describes the dissipation induced by the leakage of cavity A and cavity B, and $\hat{L}_{\gamma n} = \sqrt{\gamma} |g_n\rangle\langle e_n|$ ($n = 1, 2$), which describes the dissipation induced by the spontaneous emission of the two atoms. κ and γ are the leakage rate of the cavities and the atomic spontaneous emission rate, respectively.

Preparation of the steady entanglement. We transform the Hamiltonian H_{WL}^I in Eq. (6) back into the original picture. The spectroscopy of the system is well described by the dressed states, i.e., the eigenstates of the Hamiltonian $H_0 + H_{WL}^I$, as shown in Fig. 2(a). Note that the excitation number of the total system $N_e = \sum_{i=1,2} (|e_i\rangle\langle e_i| + c_i^\dagger c_i)$ commutes with H_0 and H_{WL}^I ; the excitation number is thus conserved under the control of these two Hamiltonians. Nevertheless, the Hamiltonian H_{CL} and Lindblad superoperator \hat{L}_j will change the excitation number because these two operators do not commute with the excitation number operator. By choosing suitable driving field frequencies, the

transitions to the Hilbert subspaces with three or more excitations are off-resonance with the two classical fields due to the unequal spacings of the energy levels of the dressed states. When the Rabi frequencies of the classical fields are substantially smaller than the atom-cavity mode coupling strength, i.e., $\Omega_1, \Omega_2 \ll g$, populations of the dressed states with more than two excitations can be neglected. Therefore, we can restrict our analysis to the physical mechanism of dissipative preparation in the Hilbert subspace up to two excitations. We denote the dressed state of the coupled system as $|A, B\rangle|C, D\rangle$, where the first and second ket represent the state of the two atoms and of the two delocalized bosonic modes, respectively. $A \in \{e_1, g_1\}$, $B \in \{e_2, g_2\}$ and $C(D) \in \{m\}$, with m being the positive integer used to denote the photon number. The dressed states $|\Phi_{N_e}\rangle$ with the corresponding eigenvalue E_{N_e} within the excitation subspace N_e can be expressed as follows: the ground state $|\Phi_0\rangle = |g_1, g_2\rangle|0, 0\rangle$ ($E_0 = 0$); the one-excitation states $|\Phi_1^0\rangle = |\phi_-\rangle|0, 0\rangle$ ($E_1^0 = \omega_0$) and $|\Phi_1^\pm\rangle = \frac{1}{\sqrt{2}}[|\phi_+\rangle|0, 0\rangle \pm |g_1, g_2\rangle|1, 0\rangle]$ ($E_1^\pm = \omega_0 \pm g$), where $|\phi_\pm\rangle = 1/\sqrt{2}(|e_1, g_2\rangle \pm |g_1, e_2\rangle)$ and $|\Phi_1^0\rangle$ is the maximal entanglement to be prepared for the two atoms; and the two-excitation states $|\Phi_2^0\rangle = |\phi_-\rangle|1, 0\rangle$ ($E_2^0 = 2\omega_0$), $|\Phi_2^1\rangle = \frac{1}{\sqrt{3}}(|g_1, g_2\rangle|2, 0\rangle - \sqrt{2}|e_1, e_2\rangle|0, 0\rangle)$ ($E_2^1 = 2\omega_0$), and $|\Phi_2^\pm\rangle = \frac{1}{\sqrt{2}}[|\phi_+\rangle|1, 0\rangle \pm \frac{1}{\sqrt{3}}(\sqrt{2}|g_1, g_2\rangle|2, 0\rangle + |e_1, e_2\rangle|0, 0\rangle)]$ ($E_2^\pm = 2\omega_0 \pm \sqrt{3}g$). These dressed states are the eigenstates of the Hamiltonian $H_0 + H_{WL}^I$, which can be considered as a set of approximately complete bases. Under the dressed state picture, the Hamiltonian H_{CL} can be rewritten as

$$\begin{aligned}
 H_{CL} = & \sum_{k=1,2} \Omega_k e^{-i\omega_k t} \left[\frac{1}{2}(|\Phi_1^- \rangle + |\Phi_1^+ \rangle)\langle\Phi_0| + \frac{1}{\sqrt{2}}|\Phi_1^0\rangle\langle\Phi_0| \right. \\
 & + \frac{1}{2\sqrt{3}}(|\Phi_2^- \rangle - |\Phi_2^+ \rangle)\langle\Phi_1^0| + \frac{1}{\sqrt{3}}|\Phi_2^1\rangle\langle\Phi_1^0| \\
 & + \left(\frac{1}{2\sqrt{6}} + \frac{1}{2\sqrt{2}} \right) |\Phi_2^+ \rangle\langle\Phi_1^+| + \frac{1}{2}|\Phi_2^0\rangle\langle\Phi_1^+| \\
 & + \left(\frac{1}{2\sqrt{2}} - \frac{1}{2\sqrt{6}} \right) |\Phi_2^- \rangle\langle\Phi_1^+| - \frac{1}{\sqrt{6}}|\Phi_2^1\rangle\langle\Phi_1^+| \\
 & + \left(\frac{1}{2\sqrt{6}} - \frac{1}{2\sqrt{2}} \right) |\Phi_2^+ \rangle\langle\Phi_1^-| - \frac{1}{2}|\Phi_2^0\rangle\langle\Phi_1^-| \\
 & \left. - \left(\frac{1}{2\sqrt{2}} + \frac{1}{2\sqrt{6}} \right) |\Phi_2^- \rangle\langle\Phi_1^-| - \frac{1}{\sqrt{6}}|\Phi_2^1\rangle\langle\Phi_1^-| + \text{H.c.} \right]. \quad (8)
 \end{aligned}$$

We proceed to the interaction picture with respect to the Hamiltonian $H_0 + H_{WL}^I$ expressed by the eigenvectors and eigenvalues in the zero-, one- and two-excitation subspaces. Eq. (8) can be rewritten as

$$\begin{aligned}
 H_{CL}^I = & \sum_{k=1,2} \Omega_k \left[\frac{1}{2}(e^{i(\Delta_k - g)t}|\Phi_1^- \rangle\langle\Phi_0| + e^{i(\Delta_k + g)t}|\Phi_1^+ \rangle\langle\Phi_0|) \right. \\
 & + e^{i\Delta_k t} \left(\frac{1}{\sqrt{2}}|\Phi_1^0\rangle\langle\Phi_0| + \frac{1}{\sqrt{3}}|\Phi_2^1\rangle\langle\Phi_1^0| \right) \\
 & + \frac{1}{2\sqrt{3}}(e^{i(\Delta_k - \sqrt{3}g)t}|\Phi_2^- \rangle\langle\Phi_1^0| - e^{i(\Delta_k + \sqrt{3}g)t}|\Phi_2^+ \rangle\langle\Phi_1^0|) \\
 & + \left(\frac{1}{2\sqrt{6}} + \frac{1}{2\sqrt{2}} \right) e^{i[\Delta_k + (\sqrt{3}-1)g]t} |\Phi_2^+ \rangle\langle\Phi_1^+| \\
 & + \left(\frac{1}{2\sqrt{2}} - \frac{1}{2\sqrt{6}} \right) e^{i[\Delta_k - (\sqrt{3}+1)g]t} |\Phi_2^- \rangle\langle\Phi_1^+| \\
 & + e^{i(\Delta_k - g)t} \left(\frac{1}{2}|\Phi_2^0\rangle\langle\Phi_1^+| - \frac{1}{\sqrt{6}}|\Phi_2^1\rangle\langle\Phi_1^+| \right) \\
 & + \left(\frac{1}{2\sqrt{6}} - \frac{1}{2\sqrt{2}} \right) e^{i[\Delta_k + (\sqrt{3}+1)g]t} |\Phi_2^+ \rangle\langle\Phi_1^-| \\
 & - \left(\frac{1}{2\sqrt{2}} + \frac{1}{2\sqrt{6}} \right) e^{i[\Delta_k - (\sqrt{3}-1)g]t} |\Phi_2^- \rangle\langle\Phi_1^-| \\
 & \left. - e^{i(\Delta_k + g)t} \left(\frac{1}{2}|\Phi_2^0\rangle\langle\Phi_1^-| + \frac{1}{\sqrt{6}}|\Phi_2^1\rangle\langle\Phi_1^-| \right) + \text{H.c.} \right]. \quad (9)
 \end{aligned}$$

By setting the detuning $\Delta_k = \omega_0 - \omega_k$ equals to $-(-1)^k g$ ($k = 1, 2$), the driving field Ω_1 resonantly drives the transitions $|\Phi_0\rangle \leftrightarrow |\Phi_1^- \rangle$, $|\Phi_1^+ \rangle \leftrightarrow |\Phi_2^0\rangle$ and $|\Phi_1^+ \rangle \leftrightarrow |\Phi_2^1\rangle$; Ω_2 resonantly drives $|\Phi_0\rangle \leftrightarrow |\Phi_1^+ \rangle$, $|\Phi_1^- \rangle \leftrightarrow |\Phi_2^0\rangle$ and $|\Phi_1^- \rangle \leftrightarrow |\Phi_2^1\rangle$; and all other transitions between any two arbitrary dressed states are largely detuned. Under the weak excitation condition, i.e., $\Omega_k \ll g$, using the rotating wave approximation, we can adiabatically eliminate the non-resonance coupling terms. The Hamiltonian H_{CL}^I reduces to

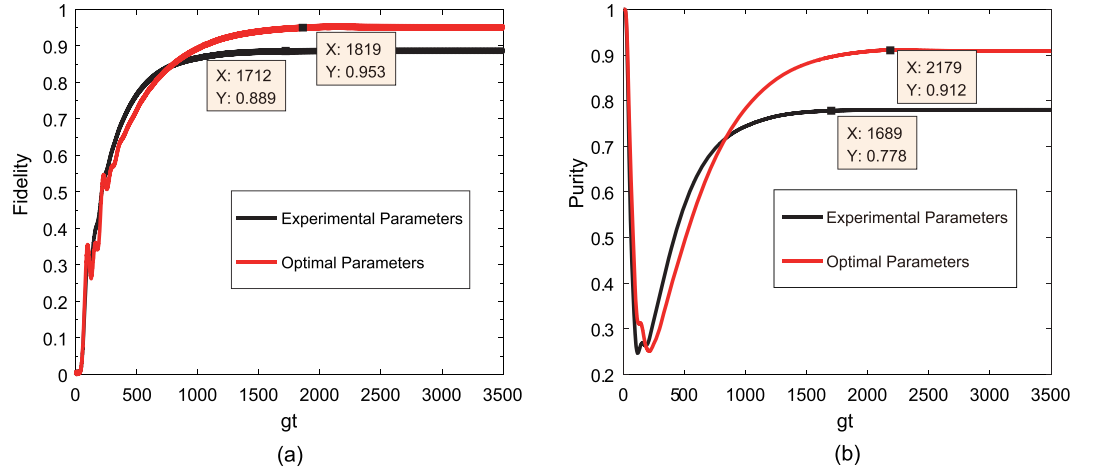


Figure 3. Fidelity (a) and purity (b) of the target state $|\Phi_0^0\rangle$ versus the dimensionless parameter gt for the initial state $|\Phi_0\rangle$ with the optimized Rabi frequencies of drivings $\Omega_1 = 0.037g$ and $\Omega_2 = 0.0775g$ and a cavity-cavity hopping strength $J = 20g$. The chosen experimental parameters are $\gamma = 2.72 \times 10^{-4}g$ and $\kappa = 2.8 \times 10^{-2}g$. In addition, the chosen optimized parameters are $\gamma = 1.75 \times 10^{-5}g$ and $\kappa = 1.6 \times 10^{-2}g$.

$$H_{CL}' = \Omega_1 \left[\frac{1}{2} |\Phi_1^-\rangle \langle \Phi_0| + \frac{1}{2} |\Phi_2^0\rangle \langle \Phi_1^+| - \frac{1}{\sqrt{6}} |\Phi_2^1\rangle \langle \Phi_1^+| \right] \\ \times \Omega_2 \left[\frac{1}{2} |\Phi_1^+\rangle \langle \Phi_0| - \frac{1}{2} |\Phi_2^0\rangle \langle \Phi_1^-| - \frac{1}{\sqrt{6}} |\Phi_2^1\rangle \langle \Phi_1^-| \right] + \text{H. c.} \quad (10)$$

From the above equation, we can see that the target state $|\Phi_0^0\rangle$ is decoupled from the Hamiltonian H_{CL}' . Hence, we can derive $-i[H_{CL}', |\Phi_0^0\rangle \langle \Phi_0^0|] = 0$. To generate the required Bell state, here, we require the atomic spontaneous emission to be much slower than other dynamical processes, i.e., $\gamma \ll \Omega_1, \Omega_2, \kappa$, so that it can be ignored, which guarantees that any transitioning away from the target state is strongly suppressed. Since $|\Phi_0^0\rangle = |\phi_-\rangle \otimes |00\rangle$ is a Kronecker product state of the Bell state and the two delocalized vacuum bosonic modes, it is unaffected by the photon decay, i.e., $\frac{1}{2} \sum_i [2\hat{L}_{\kappa i} |\Phi_1^0\rangle \langle \Phi_0^0| \hat{L}_{\kappa i}^\dagger - (\hat{L}_{\kappa i}^\dagger \hat{L}_{\kappa i} |\Phi_1^0\rangle \langle \Phi_0^0| + |\Phi_1^0\rangle \langle \Phi_0^0| \hat{L}_{\kappa i}^\dagger \hat{L}_{\kappa i})] = 0$ ($i = A, B$). Therefore, the transitions associated with the target state $|\Phi_0^0\rangle$ are hardly affected by classical drivings and cavity decay, so that it is a steady state.

The processes for producing and stabilizing the Bell state $|\Phi_0^0\rangle$ are shown in Fig. 2(b). The initial system state $|\Phi_0\rangle$ is driven by the classical field Ω_1 (Ω_2) to the one-excitation dressed state $|\Phi_1^-\rangle$ ($|\Phi_1^+\rangle$) and then to $|\Phi_2^0\rangle$ and $|\Phi_2^1\rangle$ by the classical field Ω_2 (Ω_1). The photon loss in the cavities results in the decaying channel $|\Phi_2^0\rangle \rightarrow |\Phi_1^0\rangle = |\phi_+\rangle |0, 0\rangle$. On the other hand, the state $|\Phi_2^1\rangle$ decays to the one-excitation dressed state $|\Phi_1^\pm\rangle$, being repumped by the classical fields Ω_1 and Ω_2 to $|\Phi_2^0\rangle$ and $|\Phi_2^1\rangle$; then, with the coherent driving and dissipation processes continuing, the population of the dressed state $|\Phi_2^1\rangle$ gradually declines until the entire qubit population is driven to the Bell state $|\Phi_0^0\rangle$.

Discussion

To demonstrate the feasibility of our Bell-state stabilization mechanism, we assess the performance of our scheme by numerically solving the Lindblad master equation. Under the condition that the atomic spontaneous emission rate is much slower than other dynamical processes, i.e., $\gamma \ll \kappa, \Omega_1, \Omega_2$, we choose the following parameters from a recent circuit QED experiment³⁷: $\chi/2\pi \simeq 6\text{MHz}$, $\kappa/2\pi \simeq 1.7\text{MHz}$, $T_1 \simeq 9\mu\text{s}$, where T_1 is the qubit energy relaxation time, and $\chi = g^2/\Delta$, with Δ being the qubit-resonator detuning. It is reasonable to set $\Delta = 10g$ in this dispersive interaction system, yielding $g/2\pi \simeq 60\text{MHz}$, $\kappa \simeq 2.8 \times 10^{-2}g$, and $\gamma \simeq 2.72 \times 10^{-4}g$. We have taken the optimized Rabi frequencies of the drivings $\Omega_1 = 0.037g$ and $\Omega_2 = 0.0775g$ and the cavity-cavity hopping strength $J = 20g$. In Fig. 3(a), we plot the evolutions of the fidelity $F(t) = \text{Tr}[(|\phi_+\rangle \langle \phi_+| \otimes I_c) \hat{\rho}(t \rightarrow \infty)]$ with experimental and optimized parameters. The results show that the desired state can be prepared with a fidelity greater than 88% when the evolution time $t \simeq 1712/g$. By taking $\gamma = 1.75 \times 10^{-5}g$ and $\kappa = 1.6 \times 10^{-2}g$, the optimal fidelity for the target state is approximately 95.3% when the evolution time $t \simeq 1819/g$. Dissipative processes generally lead to the production of mixed states; therefore, we introduce purity to characterize the mixture degree of the target state. With the above two sets of parameters, in Fig. 3(b), the purity $P(t) = \text{Tr}[\hat{\rho}(t)^2]$ of the target state is plotted as a function of the evolution time. The target state can be stabilized using an experimental purity of approximately 83% and an optimal purity of approximately 94%. Because the initial state of the system is $|\Phi_0\rangle$, the purity is precisely unity. In addition, note that the purity curve exhibits a valley in the regime $0 < t < 500/g$. This valley occurs because the coherent driving is dominant in the early stages of evolution, thus leading the system to be in a mixture of a variety of quantum states. With increasing evolution time, the competition between

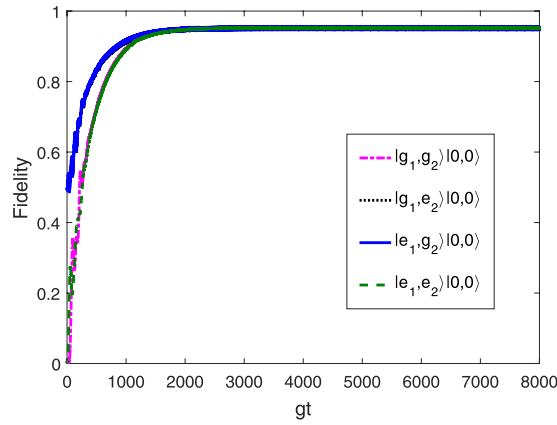


Figure 4. Fidelity of $|\Phi_1^0\rangle$, plotted versus gt for four different initial states $|g_1, g_2\rangle|0, 0\rangle$, $|g_1, e_2\rangle|0, 0\rangle$, $|e_1, g_2\rangle|0, 0\rangle$, and $|e_1, e_2\rangle|0, 0\rangle$ with the optimized parameters $\Omega_1 = 0.037g$, $\Omega_2 = 0.0775g$, $J = 20g$, $\gamma = 1.75 \times 10^{-5}g$, and $\kappa = 1.6 \times 10^{-2}g$.

the coherent driving and dissipation drives the system to a dynamic equilibrium, which is a mixture of specific dressed states.

To inspect the uniqueness of target state $|\Phi_1^0\rangle$ numerically, in Fig. 4, we show the behavior of the fidelity with respect to the target state for four different initial states $|g_1, g_2\rangle|0, 0\rangle$, $|g_1, e_2\rangle|0, 0\rangle$, $|e_1, g_2\rangle|0, 0\rangle$, and $|e_1, e_2\rangle|0, 0\rangle$. We see that for the optimized parameters $\Omega_1 = 0.037g$, $\Omega_2 = 0.0775g$, $J = 20g$, $\gamma = 1.75 \times 10^{-5}g$, and $\kappa = 1.6 \times 10^{-2}g$, any initial state can be driven to the target state asymptotically. This can be explained as follows. Consider the initial state $|e_1, g_2\rangle|0, 0\rangle$ or $|g_1, e_2\rangle|0, 0\rangle$, which can be regarded as a superposition of the one-excitation dressed states $|\Phi_1^\pm\rangle$ and $|\Phi_2^\pm\rangle$. As has been shown, due to the coherent driving and dissipation process, the populations of $|\Phi_1^\pm\rangle$ are ultimately transferred to the target steady state when the evolution time $t \simeq 1791/g$. Similarly, if the initial state is $|e_1, e_2\rangle|0, 0\rangle$, which is a specific superposition of the dressed states $|\Phi_2^\pm\rangle$ and $|\Phi_1^\pm\rangle$, the state should evolve to the states $|\phi_-\rangle|1, 0\rangle$ and $|g_1, g_2\rangle|2, 0\rangle$ induced by the coupling between the qubits and the collective photon modes. These two states continuously decay to $|\phi_-\rangle|0, 0\rangle$ and $|g_1, g_2\rangle|1, 0\rangle$ due to collective photon losses. The state $|g_1, g_2\rangle|1, 0\rangle$, which can be expanded using the dressed states $|\Phi_1^\pm\rangle$ and $|\Phi_2^\pm\rangle$, will undoubtedly be transformed into the steady entanglement state when the evolution time $t \simeq 1819/g$. Therefore, the generation of the target steady state is independent of the initial state, and every choice can lead to identical population for the target state.

The CHSH correlation $S(t)$ is defined as⁵⁵

$$S(t) = \text{Tr}[(O_{\text{CHSH}})\rho(t)], \quad (11)$$

with

$$O_{\text{CHSH}} = \sigma_{y,1} \otimes \frac{-\sigma_{y,2} - \sigma_{x,2}}{\sqrt{2}} + \sigma_{x,1} \otimes \frac{-\sigma_{y,2} - \sigma_{x,2}}{\sqrt{2}} + \sigma_{x,1} \otimes \frac{\sigma_{y,2} - \sigma_{x,2}}{\sqrt{2}} - \sigma_{y,1} \otimes \frac{\sigma_{y,2} - \sigma_{x,2}}{\sqrt{2}}, \quad (12)$$

where $\sigma_{x,1}$ ($\sigma_{x,2}$) and $\sigma_{y,1}$ ($\sigma_{y,2}$) are the Pauli operators of atom 1(2). With the above experimental parameters, the CHSH correlation versus the evolution time is plotted in Fig. 5, from which one can observe a value of approximately 2.45, clearly exceeding the maximum value of 2 allowed by local hidden variable theories.

When referring to experimental implementation, it is possible that some system parameters may be unable to maintain their preset values as expected. In Fig. 6(a,b), the fidelity and purity are plotted as functions of the Rabi frequencies Ω_1 and Ω_2 , respectively, for the given dissipative factors κ and γ . The results show that the fidelity and purity are higher than 80% and 70%, respectively, within a wide range of Rabi frequencies, demonstrating that the scheme is insensitive to deviations of the control parameters Ω_1 and Ω_2 .

To clearly observe the role of each dissipative factor, we first consider the system without spontaneous emission, and then we consider it without cavity decay. In Fig. 7(a), we plot the fidelity of the target state $|\Phi_1^0\rangle$ by taking the atomic spontaneous emission rate as $\gamma = 0$ and the cavity decay rate as $\kappa = 2.8 \times 10^{-2}g$, which shows that the desired state can be prepared with a fidelity of 94.5% and that the time for the system to reach the steady state is approximately $t = 1413/g$. This result is approximately 5% higher than that of the situation for $\gamma = 2.72 \times 10^{-4}g$ in Fig. 3(a). The inset in Fig. 7(a) shows that when the system is stabilized, i.e., when the evolution time is fixed at $t = 4 \times 10^3/g$, the fidelity decreases with increasing γ . This result occurs because as γ increases, the transition rate from the target steady state to the ground state $|\Phi_0\rangle$ becomes stronger such that the fidelity decreases. This proves that the ideal entanglement generation scheme requires the atomic spontaneous emission rate $\gamma = 0$. In Fig. 7(b), we plot the fidelity of the target state by taking the cavity decay rate as $\kappa = 0$ and the atomic spontaneous emission rate as $\gamma = 2.72 \times 10^{-4}g$. The results show that when the values of the cavity decay rate are set to zero, the scheme

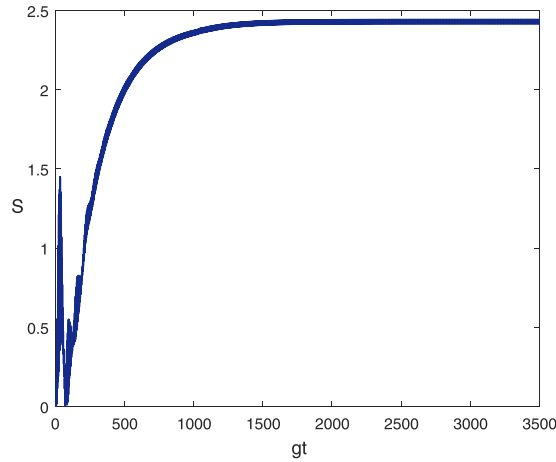


Figure 5. CHSH correlation as a function of gt for the preset parameters $\Omega_1 = 0.037g$, $\Omega_2 = 0.0775g$, and $J = 20g$. The chosen experimental dissipative factors are $\gamma = 2.72 \times 10^{-4}g$ and $\kappa = 2.8 \times 10^{-2}g$.

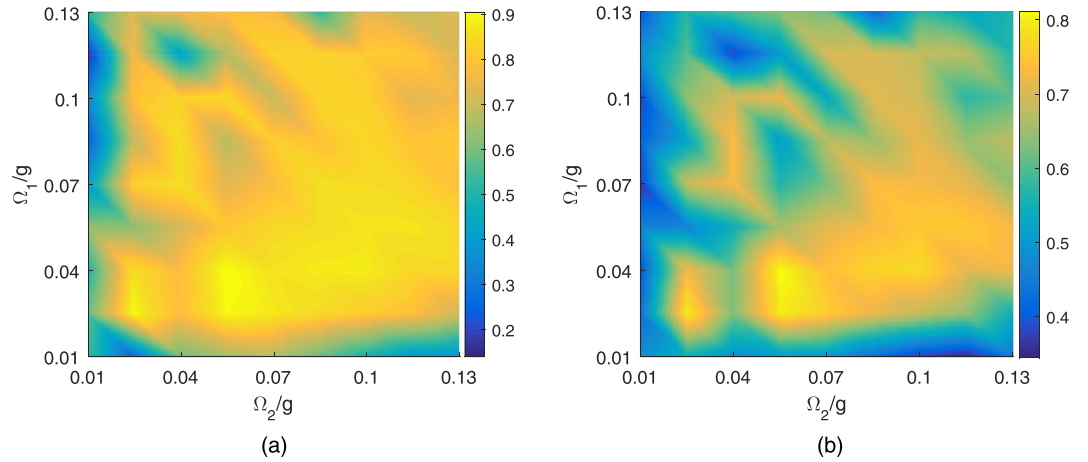


Figure 6. Fidelity (a) and purity (b) of the target state as a function of the parameters Ω_1/g and Ω_2/g with the initial state $|\Phi_0\rangle$ at the time $4 \times 10^3/g$. The chosen parameters are $\Omega_1 = 0.037g$, $\Omega_2 = 0.0775g$, $J = 20g$, $\gamma = 2.72 \times 10^{-4}g$, and $\kappa = 2.8 \times 10^{-2}g$.

cannot succeed. In the inset of Fig. 7(b), we choose the evolution time as $t = 4 \times 10^3/g$ and plot the fidelity of the presented scheme with varying cavity decay rate κ . As κ increases, the fidelity clearly increases. Nevertheless, further increases in the cavity decay will have an adverse effect on the unitary dynamics and thus decrease the overall performance of the scheme. Therefore, the results provide further verification that the ideal entanglement generation scheme can be achieved based on cavity decay.

Different from the atomic spontaneous emission, atoms are characterized by another dissipation factor: pure dephasing. This detrimental effect will be included in the numerical simulation. The Lindblad operator describing the dephasing of atom n can be written as $\hat{L}_{\gamma_\phi}^n = \sqrt{\gamma_\phi/2}(|e_n\rangle\langle e_n| - |g_n\rangle\langle g_n|)$ ($n = 1, 2$), where γ_ϕ is the atomic dephasing rate. We choose the pure dephasing time $T_\phi \simeq 36\mu\text{s}$ ($\gamma_\phi = 1/T_\phi \simeq 6.8 \times 10^{-5}g$), based on the experimental work in³⁷, and solve the master equation numerically to qualify its influence on our scheme, as shown in Fig. 8(a). We plot the fidelity and purity of the target state $|\Phi_1^0\rangle$ as functions of gt with the initial state $|\Phi_0\rangle$ by taking the optimized Rabi frequencies of the drivings as $\Omega_1 = 0.037g$ and $\Omega_2 = 0.0775g$, the cavity-cavity hopping strength as $J = 20g$, and the experimental dissipative factors as $\kappa = 2.8 \times 10^{-2}g$ and $\gamma = 2.72 \times 10^{-4}g$. After comparing Figs 3 and 8(a), one can see that the dephasing has a slight influence on the fidelity and purity, which are approximately 0.7% and 1% lower than those without consideration of the effects of dephasing, respectively. In Fig. 8(b), we consider the system in stabilization (the evolution time $t = 8 \times 10^3/g$) and plot the fidelity and purity versus the atomic dephasing rate γ_ϕ . The fidelity and purity are observed to decrease as γ_ϕ increases. When γ_ϕ changes from 0 to $1.2 \times 10^{-5}g$, the fidelity and purity are decreased only by 1.1% and 1.97%, respectively. This result occurs because atomic dephasing results in a population transfer between the singlet states $|\phi_-\rangle$ and $|\phi_+\rangle$, decreasing the fidelity and purity of the target steady state.

To further understand the proposed dissipative entanglement preparation scheme, we derive the stationary fidelity in analytical form for the target state with some reasonable approximations. First, we adiabatically

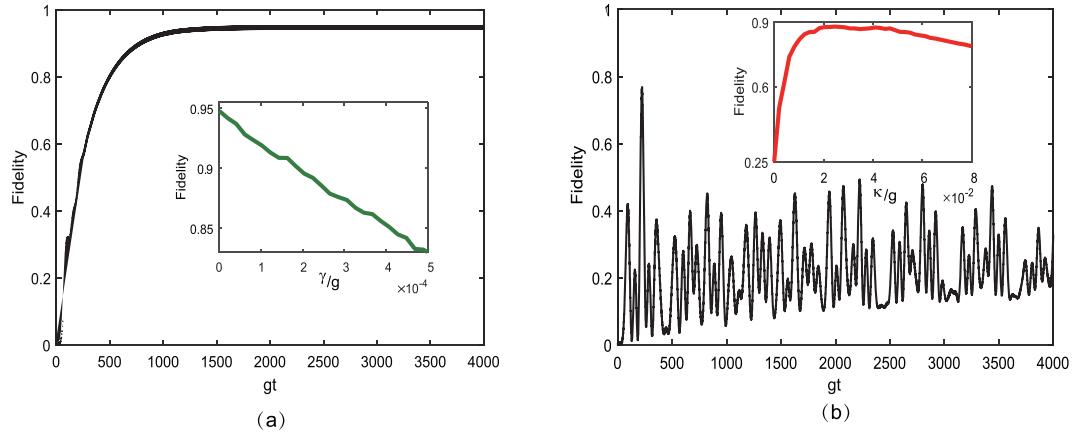


Figure 7. (a,b) Fidelity of the steady state $|\Phi_1^0\rangle$ versus gt with the initial state $|\Phi_0\rangle$. The chosen parameters are $\Omega_1 = 0.037g$, $\Omega_2 = 0.0775g$, and $J = 20g$. In (a), the selected dissipative factors are $\gamma = 0$ and $\kappa = 2.8 \times 10^{-2}g$. The inset of (a) shows the fidelity of the steady state as a function of the atomic spontaneous rate γ for the dissipative factors $\kappa = 2.8 \times 10^{-2}g$. γ varies from 0 to $5 \times 10^{-4}g$ at time $4 \times 10^3/g$. In (b), the selected dissipative factors are $\kappa = 0$ and $\gamma = 2.72 \times 10^{-4}g$. The inset of (b) shows the fidelity of the steady state as a function of the cavity decay rate κ with the dissipative factor $\gamma = 2.72 \times 10^{-4}g$. κ varies from 0 to $8 \times 10^{-2}g$ at time $4 \times 10^3/g$.

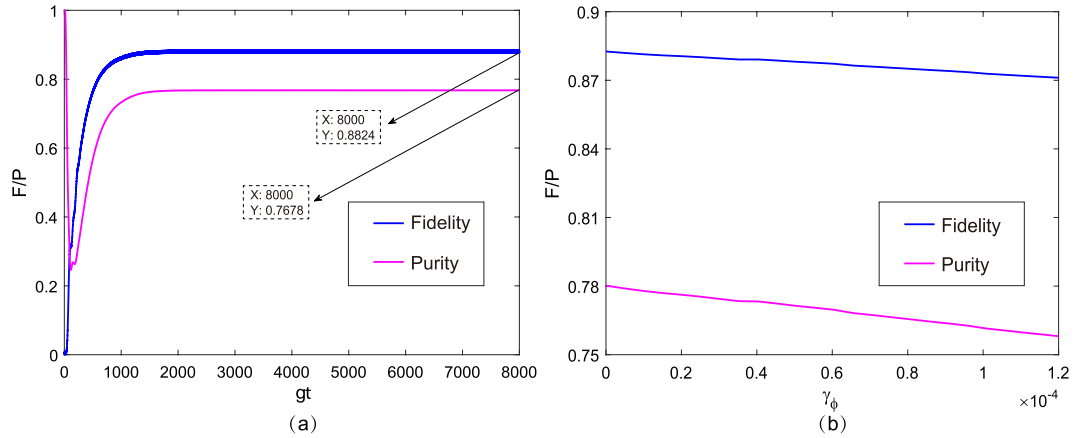


Figure 8. (a) Fidelity and purity of the steady state $|\Phi_1^0\rangle$ as a function of gt with the initial state $|\Phi_0\rangle$ when considering the effect of pure dephasing, where the selected parameters are $\Omega_1 = 0.037g$, $\Omega_2 = 0.0775g$, and $J = 20g$. We choose the experimental dissipative factors $\gamma = 2.72 \times 10^{-4}g$, $\kappa = 2.8 \times 10^{-2}g$, and $\gamma_\phi = 6.8 \times 10^{-5}g$. (b) Fidelity and purity of the steady state $|\Phi_1^0\rangle$, plotted versus the atomic dephasing rate γ_ϕ with the experimental dissipative factors $\gamma = 2.72 \times 10^{-4}g$ and $\kappa = 2.8 \times 10^{-2}g$. γ_ϕ varies from 0 to $1.2 \times 10^{-4}g$ at time $8 \times 10^3/g$.

eliminate the non-resonance coupling terms from Eq. (9) using the rotating wave approximation under the following conditions: the detuning $\Delta_k = \omega_0 - \omega_k$ is equal to $-(-1)^k g$ ($k = 1, 2$), and the weak excitation $\Omega_k \ll g$. Second, there are two processes for generating the steady entanglement $|\Phi_0\rangle \xrightarrow{\Omega_1} |\Phi_1^-\rangle \xrightarrow{\Omega_2} |\Phi_2^0\rangle \xrightarrow{\kappa} |\Phi_1^0\rangle$ and $|\Phi_0\rangle \xrightarrow{\Omega_2} |\Phi_1^+\rangle \xrightarrow{\Omega_1} |\Phi_2^0\rangle \xrightarrow{\kappa} |\Phi_1^0\rangle$. To reduce the dimensions of the system, we incorporate the same dynamical processes by eliminating the intermediate state $|\Phi_1^+\rangle$ because both processes could drive the initial state to $|\Phi_2^0\rangle$ and then decay to $|\Phi_1^0\rangle$. Therefore, we set $|\varphi_1\rangle = |\Phi_0\rangle$, $|\varphi_2\rangle = |\Phi_1^-\rangle$, $|\varphi_3\rangle = |\Phi_2^0\rangle$, $|\varphi_4\rangle = |\Phi_1^0\rangle$, and $|\varphi_5\rangle = |\Phi_1^0\rangle$, and we define $\rho_{j,k}(t) = \langle \varphi_j | \rho(t) | \varphi_k \rangle$ ($j, k = 1, 2, 3, 4, 5$), where $\rho(t)$ is the density operator of the system. Because the decays of states $|\varphi_2\rangle$, $|\varphi_3\rangle$, and $|\varphi_4\rangle$ are dominated by dissipation of the bosonic modes, we can discard the effects of atomic spontaneous emission associated with these states. With this assumption, the probability of the system being in a different state is governed by the stationary state equation $d\rho_{j,k}(t)/dt = 0$. By analytically solving the Lindblad master equation, we can obtain the diagonal elements of the five-dimensional density matrix (see the Methods subsection for the detailed calculation). Because the 25 stationary state equations are algebraic equations, we do not need to introduce a preset initial state, in contrast to the differential equations, which require presetting a certain initial state. Therefore, the stationary solutions have a generality in indirectly verifying the uniqueness of $|\Phi_1^0\rangle$, i.e., arbitrary initial states can be driven to the target state $|\Phi_1^0\rangle$, which leads to the target state having an identical fidelity. This is in agreement with the numerical simulation in Fig. 4. To assess the accuracy of

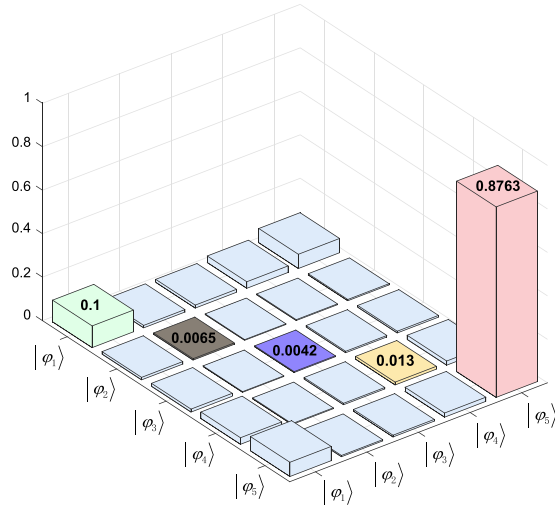


Figure 9. Truth table of the steady-state density matrix. The parameters used are $\kappa = 2 \times 2.8 \times 10^{-2} g$ and $\gamma = 2.72 \times 10^{-4} g$, and the optimized Rabi frequencies of the drivings are $\Omega_1 = 0.037 g$ and $\Omega_2 = 0.0775 g$.

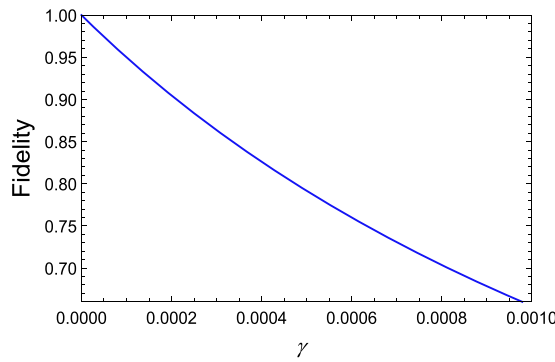


Figure 10. Fidelity of the target steady state as a function of the atomic spontaneous emission rate.

the approximate analytical solution, we take the experimental parameters $\kappa = 2 \times 2.8 \times 10^{-2} g$ and $\gamma = 2.72 \times 10^{-4} g$ and the optimized Rabi frequencies of the drivings $\Omega_1 = 0.037 g$ and $\Omega_2 = 0.0775 g$. Here, κ is the collective bosonic mode decay; it is reasonable to select a value of twice the leakage of the cavity field. In Fig. 9, we present a truth table of the steady-state density matrix constructed corresponding to the analytical results; the table indicates that the fidelity of the target steady state is approximately $\rho_{5,5} = 0.8763$. This is only slightly different from the numerical fidelity of 0.889 for the initial state $|\Phi_0\rangle$. Note that the approximation is valid under the condition that spontaneous emission is a passive source in driving the atomic qubits out of the target steady state. In Fig. 10, the fidelity of the target steady state is plotted as a function of the atomic spontaneous emission rate γ . The result shows that the fidelity decreases as the atomic spontaneous emission rate increases to a bearable extent; further increases in the dissipative factors will have greater negative effects on the performance of the scheme. In addition, to analytically verify the stationarity of the target entangled state $|\Phi_1^0\rangle$, we consider an ideal (the spontaneous emission rate $\gamma = 0$) and effective ($|\Phi_0\rangle \xleftrightarrow{\Omega} |\Phi_2^0\rangle \xleftrightarrow{\kappa} |\Phi_1^0\rangle$) process. At this point, the density operator $\rho(t)$ of the system becomes 3×3 . The initial state of the system is assumed to be $|\Phi_0\rangle$; thus, we can analytically give

$$d\rho_{5,5}(t)/dt = \frac{16e^{-\frac{t\kappa}{2}}\Omega^2\kappa \text{Sinh}^2\left(\frac{1}{4}t\sqrt{\kappa^2 - 16\Omega^2}\right)}{\kappa^2 - 16\Omega^2}, \tag{13}$$

and

$$\rho_{5,5}(t) = \frac{1}{2(Q)^{3/2}}e^{-\frac{t\kappa}{2}}\left[2e^{\frac{t\kappa}{2}}(Q)^{3/2} + e^{-\frac{\sqrt{Q}t}{2}}\kappa(Q - \sqrt{Q}\kappa) + 32\sqrt{Q}\Omega^2 - e^{\frac{\sqrt{Q}t}{2}}\kappa[\kappa(\sqrt{Q} + \kappa) - 16\Omega^2]\right], \tag{14}$$

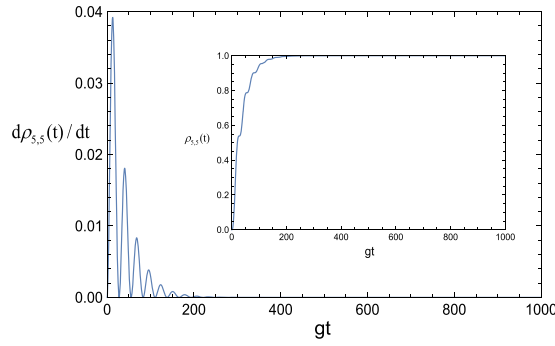


Figure 11. Variation rate of the probability for the target state versus gt with the initial state $|\Phi_0\rangle$. The chosen parameter is $\Omega = \Omega_1 + \Omega_2$, in which $\Omega_1 = 0.037g$ and $\Omega_2 = 0.0775g$. The selected dissipative factor is $\kappa = 2 \times 2.8 \times 10^{-2}g$. The inset shows the probability of the target state as a function of gt .

$Q = \kappa^2 - 16\Omega^2$ and Ω reprwhere the parameteresents the effective Rabi frequency that directly drives the transition between $|\Phi_0\rangle$ and $|\Phi_2^0\rangle$. In Fig. 11, we plot the time evolution of $d\rho_{5,5}(t)/dt$ with Eq. (13) by taking the parameter $\Omega = \Omega_1 + \Omega_2 = 0.1145g$ and the dissipative factor $\kappa = 2 \times 2.8 \times 10^{-2}g$, which exhibits an oscillatory behavior before $d\rho_{5,5}(t)/dt$ approaches 0 as the interaction time increases. This is the result of the competition between the coherent driving and dissipation. $d\rho_{5,5}(t)/dt = 0$ means that the probability of the target state reaching stabilization is time invariant. We also plot the probability of the target state versus gt in the inset of Fig. 11, which shows a very good agreement with the variance of $d\rho_{5,5}(t)/dt$.

As a practical application of our dissipative entanglement preparation scheme in quantum communication, we construct a quantum state transfer setup with multiple nodes, as shown in Fig. 12. Suppose that each node is initially prepared in the entangled steady state $|\phi_+\rangle$, which is shared by the sender (Alice) and the receiver (Bob). The unknown quantum state (referred to as a) to be transferred in Alice’s hands is $|\varphi\rangle_a = \alpha|0\rangle_a + \beta|1\rangle_a$, where α and β are unknown parameters, with $|\alpha|^2 + |\beta|^2 = 1$. Using a standard teleportation procedure^{56,57}, Bob can deterministically recover the unknown state only by applying some local operations (I_2 , σ_{x_2} , σ_{z_2} , and $\sigma_{x_2}\sigma_{z_2}$) to atom 2. In the following, the atomic state at Bob’s side is an unknown quantum state, which can be subsequently transferred from the first node to the n th node by performing the same operation.

In summary, we have proposed a scheme for producing and stabilizing a Bell state in a coupled cavity system via cavity decay. The distinct feature of our scheme is that only one atom needs to be driven by classical control fields. This not only greatly simplifies the experimental implementation between separate nodes of a quantum network but also makes the scheme robust against drive amplitude fluctuations and cavity field decay. Using the presently available experimental parameters, a steady Bell state with a high fidelity and purity can be obtained by optimizing the driving amplitudes. We have also given an analytical solution for the stationary fidelity to demonstrate the validity of our scheme, which is highly consistent with the numerical solution because we simply consider the five-dimensional subspace in the dressed state picture. Furthermore, as a practical application, we have constructed a quantum state transfer scheme with multiple nodes based our basic model. The above analysis and numerical simulations show that the present scheme is feasible with the current technology and is generally suitable for different qubit-resonator systems.

Methods

We express the density operator $\rho(t)$ of the system using the five basis states $|\varphi_1\rangle = |\Phi_0\rangle$, $|\varphi_2\rangle = |\Phi_1^-\rangle$, $|\varphi_3\rangle = |\Phi_2^0\rangle$, $|\varphi_4\rangle = |\Phi_2^1\rangle$, and $|\varphi_5\rangle = |\Phi_1^0\rangle$ and assume that the state of the system at arbitrary time t is $|\psi(t)\rangle = c_1(t)|\varphi_1\rangle + c_2(t)|\varphi_2\rangle + c_3(t)|\varphi_3\rangle + c_4(t)|\varphi_4\rangle + c_5(t)|\varphi_5\rangle$, where c_i ($i = 1, 2, 3, 4, 5$) denotes the probability amplitudes for the corresponding states. Hence, the density operator of the system in matrix form is given by

$$\rho(t) = \begin{bmatrix} |c_1(t)|^2 & c_1(t)c_2^*(t) & c_1(t)c_3^*(t) & c_1(t)c_4^*(t) & c_1(t)c_5^*(t) \\ c_2(t)c_1^*(t) & |c_2(t)|^2 & c_2(t)c_3^*(t) & c_2(t)c_4^*(t) & c_2(t)c_5^*(t) \\ c_3(t)c_1^*(t) & c_3(t)c_2^*(t) & |c_3(t)|^2 & c_3(t)c_4^*(t) & c_3(t)c_5^*(t) \\ c_4(t)c_1^*(t) & c_4(t)c_2^*(t) & c_4(t)c_3^*(t) & |c_4(t)|^2 & c_4(t)c_5^*(t) \\ c_5(t)c_1^*(t) & c_5(t)c_2^*(t) & c_5(t)c_3^*(t) & c_5(t)c_4^*(t) & |c_5(t)|^2 \end{bmatrix}, \tag{15}$$

in which the diagonal elements represent the probability, also known as the fidelity, of the corresponding states. We define $\rho_{j,k}(t) = c_j(t)c_k^*(t)$ ($j, k = 1, 2, 3, 4, 5$). The evolution of the system is described by the following coupled differential equations for the corresponding density matrix elements:

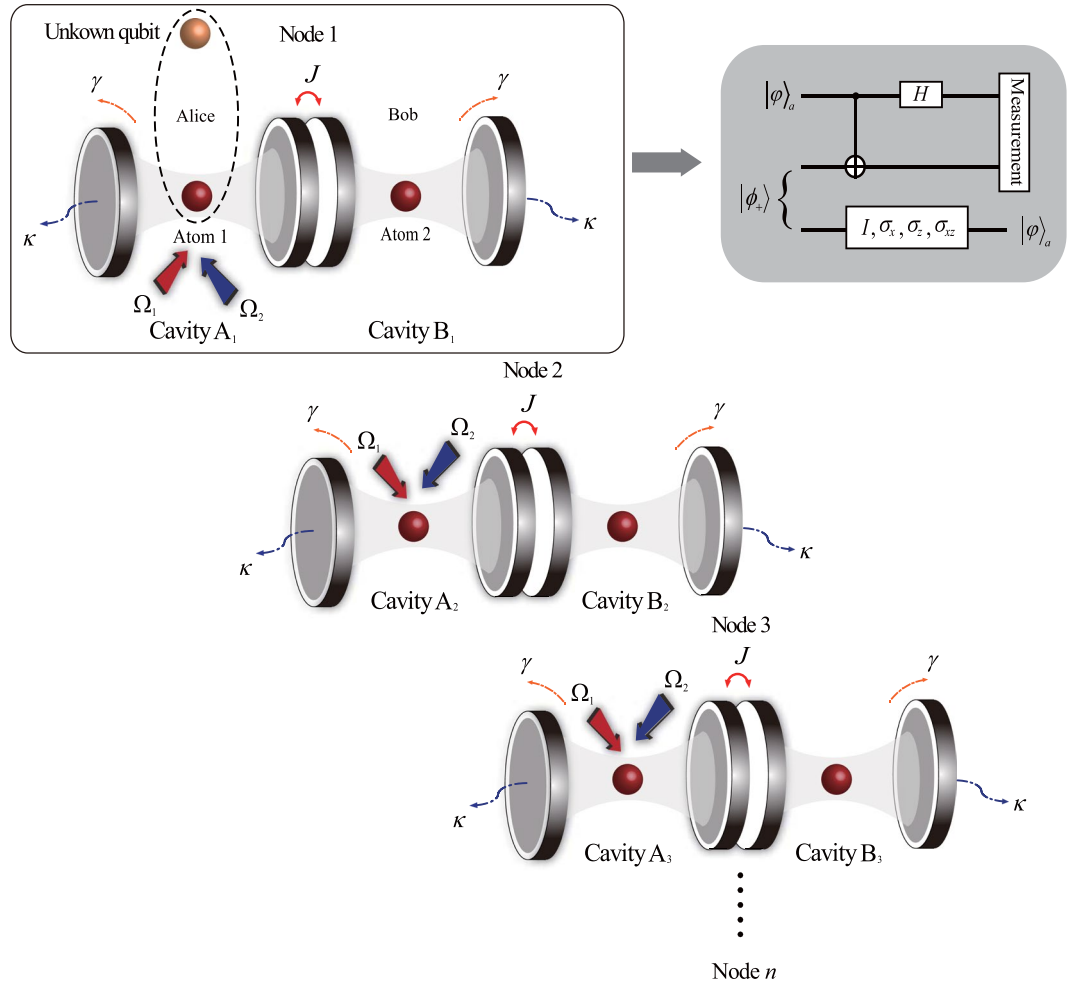


Figure 12. Schematic diagram for the implementation of quantum state transfer using a standard teleportation procedure. The information of the unknown qubit can be transferred from the first node to the n th node. The solid box denotes the first node to teleport an unknown quantum state from Alice to Bob. The dashed box in the first panel represents two qubits that belong to the same participant. The gray box to the upper right is a quantum circuit of teleportation for the first node. Here, H represents a Hadamard operation, σ_x and σ_z are the Pauli operators representing local qubit-flip operations, and I is the identity operator.

$$\begin{aligned}
 d\rho_{1,1}(t)/dt &= \frac{1}{2}[i\Omega_1(\rho_{1,2}(t) - \rho_{2,1}(t)) + \kappa\rho_{2,2}(t) + 2\gamma\rho_{5,5}(t)], \\
 d\rho_{1,2}(t)/dt &= -\frac{1}{4}\kappa\rho_{1,2}(t) - \frac{1}{2}i\Omega_2\left(\rho_{1,3}(t) + \frac{\sqrt{6}}{3}\rho_{1,4}(t)\right) \\
 &\quad + \frac{1}{2}i\Omega_1(\rho_{1,1}(t) - \rho_{2,2}(t)) + \frac{\sqrt{6}}{6}\kappa\rho_{2,4}(t), \\
 d\rho_{1,3}(t)/dt &= -\frac{1}{2}i(\Omega_2\rho_{1,2}(t) - i\kappa\rho_{1,3}(t) + \Omega_1\rho_{2,3}(t)), \\
 d\rho_{1,4}(t)/dt &= -\frac{1}{6}i\left(\sqrt{6}\Omega_2\rho_{1,2}(t) - i\kappa\rho_{1,4}(t) + 3\Omega_1\rho_{2,4}(t)\right), \\
 d\rho_{1,5}(t)/dt &= -\frac{1}{2}\gamma\rho_{1,5}(t) - \frac{\sqrt{2}}{2}\kappa\rho_{2,3}(t) - \frac{1}{2}i\Omega_1\rho_{2,5}(t), \\
 d\rho_{2,2}(t)/dt &= -\frac{1}{2}i\Omega_1(\rho_{1,2}(t) - \rho_{2,1}(t)) - \kappa(3\rho_{2,2}(t) - 2\rho_{4,4}(t)) \\
 &\quad - \frac{1}{6}i\Omega_2\left(3\rho_{2,3}(t) + \sqrt{6}\rho_{2,4}(t) - 3\rho_{3,2}(t) - \sqrt{6}\rho_{4,2}(t)\right),
 \end{aligned} \tag{16}$$

$$\begin{aligned}
d\rho_{2,3}(t)/dt &= -\frac{1}{2}i\Omega_1\rho_{1,3}(t) - \frac{3}{4}\kappa\rho_{2,3}(t) \\
&\quad - \frac{1}{6}i\Omega_2(3\rho_{2,2}(t) - 3\rho_{3,3}(t) - \sqrt{6}\rho_{4,3}(t)), \\
d\rho_{2,4}(t)/dt &= -\frac{1}{2}i\Omega_1\rho_{1,4}(t) - \frac{5}{12}\kappa\rho_{2,4}(t) \\
&\quad - \frac{1}{6}i\Omega_2(\sqrt{6}\rho_{2,2}(t) - 3\rho_{3,4}(t) - \sqrt{6}\rho_{4,4}(t)), \\
d\rho_{2,5}(t)/dt &= -\frac{1}{2}i\Omega_1\rho_{1,5}(t) - \kappa\left(\frac{1}{4}\rho_{2,5}(t) + \frac{\sqrt{3}}{3}\rho_{4,3}(t)\right) \\
&\quad + i\Omega_2\left(\frac{1}{2}\rho_{3,5}(t) + \frac{\sqrt{6}}{6}\rho_{4,5}(t)\right), \\
d\rho_{3,3}(t)/dt &= \frac{1}{2}i\Omega_2(\rho_{2,3}(t) - \rho_{3,2}(t)) - \kappa\rho_{3,3}(t), \\
d\rho_{3,4}(t)/dt &= i\Omega_2\left(\frac{1}{2}\rho_{2,4}(t) - \frac{\sqrt{6}}{6}\rho_{3,2}(t)\right) - \frac{2}{3}\kappa\rho_{3,4}(t), \\
d\rho_{3,5}(t)/dt &= \frac{1}{2}i\Omega_2\rho_{2,5}(t) - \frac{1}{2}\kappa\rho_{3,5}(t), \\
d\rho_{4,4}(t)/dt &= \frac{\sqrt{6}}{6}i\Omega_2(\rho_{2,4}(t) - \rho_{4,2}(t)) - \frac{1}{3}\kappa\rho_{4,4}(t), \\
d\rho_{4,5}(t)/dt &= \frac{1}{6}(i\Omega_2\sqrt{6}\rho_{2,5}(t) - \kappa\rho_{4,5}(t)), \\
d\rho_{5,5}(t)/dt &= \kappa\rho_{3,3}(t) - \gamma\rho_{5,5}(t),
\end{aligned}$$

in which we have omitted the corresponding transposed-conjugate terms because $d\rho_{j,k}/dt = [d\rho_{k,j}/dt]^\dagger$ ($k \neq j$). The analytical solutions for the stationary state equation $d\rho_{j,k}/dt = 0$ can be obtained as follows:

$$\begin{aligned}
\rho_{1,1} &= \frac{\gamma}{M}[288\Omega_1^6 + 160\kappa^2\Omega_1^3\Omega_2 + 8\Omega_1^4(73\kappa^2 - 9\Omega_2^2) \\
&\quad + 8\Omega_1(30\kappa^4\Omega_2 + 37\kappa^2\Omega_2^3) \\
&\quad + (\kappa^2 + 6\Omega_2^2)(30\kappa^4 + 169\kappa^2\Omega_2^2 + 198\Omega_2^4) \\
&\quad + \Omega_1^2(248\kappa^4 + 682\kappa^2\Omega_2^2 + 984\Omega_2^4)], \\
\rho_{2,2} &= \frac{4\gamma\Omega_1^2}{M}[30\kappa^4 + 72\Omega_1^4 + 109\kappa^2\Omega_2^2 \\
&\quad + 60\Omega_2^4 + 2\Omega_1^2(64\kappa^2 + 51\Omega_2^2)], \\
\rho_{3,3} &= \frac{12\gamma\Omega_1^2\Omega_2^2}{M}(10\kappa^2 + 36\Omega_1^2 + 23\Omega_2^2), \\
\rho_{4,4} &= \frac{24\gamma\Omega_1^2\Omega_2^2}{M}(30\kappa^2 + 20\Omega_1^2 + 37\Omega_2^2), \\
\rho_{5,5} &= \frac{12\kappa\Omega_1^2\Omega_2^2}{M}(10\kappa^2 + 36\Omega_1^2 + 23\Omega_2^2),
\end{aligned} \tag{17}$$

where the parameter

$$\begin{aligned}
M &= 576\gamma\Omega_1^6 + 160\gamma\kappa^2\Omega_1^3\Omega_2 + 8\gamma\kappa^2\Omega_1\Omega_2(30\kappa^2 + 37\Omega_2^2) \\
&\quad \times 8\Omega_1^4[137\gamma\kappa^2 + 6\Omega_2^2(26\gamma + 9\kappa)] \\
&\quad + \gamma(\kappa^2 + 6\Omega_2^2)(30\kappa^4 + 169\kappa^2\Omega_2^2 + 198\Omega_2^4) \\
&\quad \times 2\Omega_1^2[184\gamma\kappa^4 + \kappa^2\Omega_2^2(979\gamma + 60\kappa) + 6\Omega_2^4(199\gamma + 23\kappa)].
\end{aligned} \tag{18}$$

References

1. Einstein, A., Podolsky, B. & Rosen, N. Can quantum-mechanical description of physical reality be considered complete? *Phys. Rev.* **47**, 777 (1935).
2. Schrödinger, E. Die gegenwärtige situation in der quantenmechanik. *Naturwissenschaften* **23**, 823 (1935).
3. Simon, C. & Irvine, W. T. M. Robust long-distance entanglement and a loophole-free bell test with ions and photons. *Phys. Rev. Lett.* **91**, 110405 (2003).
4. Cirac, J. I., Zoller, P., Kimble, H. J. & Mabuchi, H. Quantum state transfer and entanglement distribution among distant nodes in a quantum network. *Phys. Rev. Lett.* **78**, 3221 (1997).
5. Deng, F. G. Efficient multipartite entanglement purification with the entanglement link from a subspace. *Phys. Rev. A* **84**, 052312 (2011).
6. Bennett, C. H. *et al.* Purification of noisy entanglement and faithful teleportation via noisy channels. *Phys. Rev. Lett.* **76**, 722 (1996).

7. Briegel, H.-J., Dür, W., Cirac, J. I. & Zoller, P. Quantum repeaters: the role of imperfect local operations in quantum communication. *Phys. Rev. Lett.* **81**, 5932 (1998).
8. Wang, T. J., Song, S. Y. & Long, G. L. Quantum repeater based on spatial entanglement of photons and quantum-dot spins in optical microcavities. *Phys. Rev. A* **85**, 062311 (2012).
9. Plenio, M. B., Huelga, S. F., Beige, A. & Knight, P. L. Cavity-loss-induced generation of entangled atoms. *Phys. Rev. A* **59**, 2468 (1999).
10. Cabrillo, C., Cirac, J. I., García-Fernández, P. & Zoller, P. Creation of entangled states of distant atoms by interference. *Phys. Rev. A* **59**, 1025 (1999).
11. Kastoryano, M. J., Reiter, F. & Sørensen, A. S. Dissipative preparation of entanglement in optical cavities. *Phys. Rev. Lett.* **106**, 090502 (2011).
12. Shen, L. T., Chen, X. Y., Yang, Z. B., Wu, H. Z. & Zheng, S. B. Steady-state entanglement for distant atoms by dissipation in coupled cavities. *Phys. Rev. A* **84**, 064302 (2011).
13. Shen, L. T., Chen, X. Y., Yang, Z. B., Wu, H. Z. & Zheng, S. B. Distributed entanglement induced by dissipative bosonic media. *Europhys. Lett.* **99**, 20003 (2012).
14. Reiter, F., Kastoryano, M. J. & Sørensen, A. S. Driving two atoms in an optical cavity into an entangled steady state using engineered decay. *New J. Phys.* **14**, 053022 (2012).
15. Busch, J. *et al.* Cooling atom-cavity systems into entangled states. *Phys. Rev. A* **84**, 022316 (2011).
16. Memarzadeh, L. & Mancini, S. Stationary entanglement achievable by environment-induced chain links. *Phys. Rev. A* **83**, 042329 (2011).
17. Vollbrecht, K. G. H., Muschik, C. A. & Cirac, J. I. Entanglement distillation by dissipation and continuous quantum repeaters. *Phys. Rev. Lett.* **107**, 120502 (2011).
18. Alharbi, A. F. & Ficek, Z. Deterministic creation of stationary entangled states by dissipation. *Phys. Rev. A* **82**, 054103 (2010).
19. Angelakis, D. G., Bose, S. & Mancini, S. Steady state entanglement between hybrid light-matter qubits. *Europhys. Lett.* **85**, 20007 (2009).
20. Braun, D. Creation of entanglement by interaction with a common heat bath. *Phys. Rev. Lett.* **89**, 277901 (2002).
21. Benatti, F., Floreanini, R. & Piani, M. Environment induced entanglement in markovian dissipative dynamics. *Phys. Rev. Lett.* **91**, 070402 (2003).
22. Benatti, F. & Floreanini, R. Entangling oscillators through environment noise. *J. Phys. A* **39**, 2689 (2006).
23. Horhammer, C. & Buttner, H. Environment-induced two-mode entanglement in quantum Brownian motion. *Phys. Rev. A* **77**, 042305 (2008).
24. Diehl, S. *et al.* Quantum states and phases in driven open quantum systems with cold atoms. *Nat. Phys.* **4**, 878 (2008).
25. Verstraete, F., Wolf, M. M. & Cirac, J. I. Quantum computation, quantum state engineering, and quantum phase transitions driven by dissipation. *Nat. Phys.* **5**, 633 (2009).
26. Vacanti, G. & Beige, A. Cooling atoms into entangled states. *New J. Phys.* **11**, 083008 (2009).
27. Shen, L. T., Chen, X. Y., Yang, Z. B., Wu, H. Z. & Zheng, S. B. Cooling distant atoms into steady entanglement via coupled cavities. *Quantum Inf. Comput.* **13**, 281 (2013).
28. Shen, L. T., Chen, X. Y., Yang, Z. B., Wu, H. Z. & Zheng, S. B. Preparation of two-qubit steady entanglement through driving a single qubit. *Optics Letters* **39**, 6046 (2014).
29. Su, S. L., Shao, X. Q., Wang, H. F. & Zhang, S. Scheme for entanglement generation in an atom-cavity system via dissipation. *Phys. Rev. A* **90**, 054302 (2014).
30. Su, S. L., Shao, X. Q., Wang, H. F. & Zhang, S. Preparation of three-dimensional entanglement for distant atoms in coupled cavities via atomic spontaneous emission and cavity decay. *Sci. Rep.* **4**, 7566 (2014).
31. Su, S. L., Guo, Q., Wang, H. F. & Zhang, S. Simplified scheme for entanglement preparation with Rydberg pumping via dissipation. *Phys. Rev. A* **92**, 022328 (2015).
32. Su, S. L. *et al.* Preparation of entanglement between atoms in spatially separated cavities via fiber loss. *Eur. Phys. J. D* **69**, 123 (2015).
33. Bhaktavatsala Rao, D. D. & Mlmer, K. Dark entangled steady states of interacting rydberg atoms. *Phys. Rev. Lett.* **111**, 033606 (2013).
34. Carr, A. W. & Saffman, M. Preparation of entangled and antiferromagnetic states by dissipative rydberg pumping. *Phys. Rev. Lett.* **111**, 033607 (2013).
35. Lin, Y. *et al.* Dissipative production of a maximally entangled steady state of two quantum bits. *Nature (London)* **504**, 415 (2013).
36. Barreiro, J. T. *et al.* An open-system quantum simulator with trapped ions. *Nature (London)* **470**, 486 (2011).
37. Shankar, S. *et al.* Autonomously stabilized entanglement between two superconducting quantum bits. *Nature* **504**, 419 (2013).
38. Reiter, F., Tornberg, L., Johansson, G. & Sørensen, A. S. Steady-state entanglement of two superconducting qubits engineered by dissipation. *Phys. Rev. A* **88**, 032317 (2013).
39. Sweke, R., Sinayskiy, I. & Petruccione, F. Dissipative preparation of large W states in optical cavities. *Phys. Rev. A* **87**, 042323 (2013).
40. Zheng, S. B. & Shen, L. T. Generation and stabilization of maximal entanglement between two atomic qubits coupled to a decaying resonator. *J. Phys. B: At. Mol. Opt. Phys.* **47**, 055502 (2014).
41. Dalla Torre, E. G., Otterbach, J., Demler, E., Vuletic, V. & Lukin, M. D. Dissipative preparation of spin squeezed atomic ensembles in a steady state. *Phys. Rev. Lett.* **110**, 120402 (2013).
42. Vasilyev, D. V. & Muschik, C. A. & Hammerer, K. Dissipative versus conditional generation of Gaussian entanglement and spin squeezing. *Phys. Rev. A* **87**, 053820 (2013).
43. Zheng, S. B. Dissipation-induced geometric phase for an atom trapped in an optical cavity. *Phys. Rev. A* **85**, 052106 (2012).
44. Wu, Q. C. *et al.* Improving the stimulated Raman adiabatic passage via dissipative quantum dynamics. *Opt. Express* **24**, 22847 (2016).
45. Song, J., Di, J. Y., Yan, X., Sun, X. D. & Jiang, Y. Y. Implementation of quantum state manipulation in a dissipative cavity. *Sci. Rep.* **5**, 10656 (2015).
46. Song, J., Xia, Y. & Song, H. S. One-step generation of cluster state by adiabatic passage in coupled cavities. *Appl. Phys. Lett.* **96**, 071102 (2010).
47. Ogden, C. D., Irish, E. K. & Kim, M. S. Dynamics in a coupled-cavity array. *Phys. Rev. A* **78**, 063805 (2008).
48. Hartmann, M. J., Brandão, F. G. S. L. & Plenio, M. B. Quantum many-body phenomena in coupled cavity arrays. *Laser Photon. Rev.* **2**, 527 (2008).
49. Di Fidio, C. & Vogel, W. Entanglement signature in the mode structure of a single photon. *Phys. Rev. A* **79**, 050303(R) (2009).
50. Cho, J., Angelakis, D. G. & Bose, S. Heralded generation of entanglement with coupled cavities. *Phys. Rev. A* **78**, 022323(R) (2008).
51. Angelakis, D. G., Santos, M. F. & Bose, S. Photon-blockade-induced Mott transitions and XY spin models in coupled cavity arrays. *Phys. Rev. A* **76**, 031805(R) (2007).
52. Hartmann, M. J., Brandão, F. G. S. L. & Plenio, M. B. Strongly interacting polaritons in coupled arrays of cavities. *Nat. Phys.* **2**, 849–855 (2006).
53. Greentree, A. D., Tahan, C., Cole, J. H. & Hollenberg, L. C. L. Quantum phase transitions of light. *Nat. Phys.* **2**, 856–861 (2006).
54. Armani, D. K., Kippenberg, T. J., Spillane, S. M. & Vahala, K. J. Ultra-high-Q toroid microcavity on a chip. *Nature(London)* **421**, 925–928 (2003).
55. Clauser, J. F., Horne, M. A., Shimony, A. & Holt, R. A. Proposed experiment to test local hidden-variable theories. *Phys. Rev. Lett.* **23**, 880 (1969).
56. Bennett, C. H. *et al.* Teleporting an unknown quantum state via dual classical and Einstein-Podolsky-Rosen channels. *Phys. Rev. Lett.* **70**, 1895 (1993).
57. Brassard, G., Braunstein, S. L. & Cleve, R. Teleportation as a quantum computation. *Physica D* **120**, 43 (1998).

Acknowledgements

This work was supported by the National Natural Science Foundations of China under Grant Nos 11564041, 11165015, 11264042, 11465020, and 61465013; the Project of Jilin Science and Technology Development for Leading Talent of Science and Technology Innovation in Middle and Young and Team Project under Grant No. 20160519022JH; the Young Teacher Startup Foundation of Zhengzhou University under Grant No. 32210411; and the China Postdoctoral Science Foundation under Grant No. 2017M612411; and the Education Department Foundation of Henan Province Under Grant No. 18A140009.

Author Contributions

J.Z., S.-L.S. and S.Z. designed the scheme and performed the simulations for the model. A.-D.Z. created the initial draft of the manuscript. All authors contributed to the interpretation of the work and the writing of the manuscript. All authors reviewed the manuscript.

Additional Information

Competing Interests: The authors declare that they have no competing interests.

Publisher's note: Springer Nature remains neutral with regard to jurisdictional claims in published maps and institutional affiliations.



Open Access This article is licensed under a Creative Commons Attribution 4.0 International License, which permits use, sharing, adaptation, distribution and reproduction in any medium or format, as long as you give appropriate credit to the original author(s) and the source, provide a link to the Creative Commons license, and indicate if changes were made. The images or other third party material in this article are included in the article's Creative Commons license, unless indicated otherwise in a credit line to the material. If material is not included in the article's Creative Commons license and your intended use is not permitted by statutory regulation or exceeds the permitted use, you will need to obtain permission directly from the copyright holder. To view a copy of this license, visit <http://creativecommons.org/licenses/by/4.0/>.

© The Author(s) 2017